Contribution from the Departments of Chemistry, The University of North Carolina, Chapel Hill, North Carolina 27599-3290, The University of Michigan, Ann Arbor, Michigan 48105-1055, and Aristotelian University of Thessaloniki, Thessaloniki, Greece

Cationic Control of Spin Dimensionality in Infinite Chains of $(Cation)_2[Mn^{III}(salicylate)_2(CH_3OH)_2][Mn^{III}(salicylate)_2]$

Martin L. Kirk,[1a] Myoung Soo Lah,[1b] Catherin Raptopoulou,[1c] Dimitris P. Kessissoglou,[1b,c] William E. Hatfield,*[,1a] and Vincent L. Pecoraro*[,1b]

Received January 15, 1991

X-ray structure analysis demonstrates that alternating AB type chains of general composition $(cat)_2[Mn^{III}(sal)_2(CH_3OH)_2][Mn^{III}(sal)_2]$ [cat = Na^+ (**1**), K^+ (**2**), NH_4^+ (**3**); sal = salicylate] can be prepared by the reaction of $MnCl_2$ with salicylic acid and the appropriate base. The molecular structures are composed of three parts: (i) the polyhedron of Mn1 in $Mn^{III}(sal)_2(CH_3OH)_2$ (the A unit), (ii) the polyhedron of Mn2 in $Mn^{III}(sal)_2$ (the B unit), which is bridged to the A structure by two carboxylates, and (iii) the monovalent cation coordination environment. Varying the cation causes increases in Mn1-Mn2 separations (Na^+, 5.347 Å; K^+, 5.520 Å; NH_4^+, 5.561 Å) and relative tilting of the tetragonal planes of the two metals [Mn2-O3-C7 angles: Na^+, 134.3 (4)°; K^+, 139.8 (3)°; NH_4^+, 140.3 (2)°]. Variable-temperature magnetic susceptibilities of **1-3** were measured to determine the type and magnitude of magnetic exchange in these $S = 2$ chains. The exchange interaction is weakly antiferromagnetic, with all three salts behaving as one-dimensional magnets and the Na^+ salt showing three-dimensional exchange. The observations are rationalized by a spin-exchange model. Crystal data are as follows. **1**: triclinic, $P\bar{1}$, a = 7.725 (2) Å, b = 10.596 (3) Å, c = 12.892 (3) Å, α = 102.75 (2)°, β = 104.64 (2)°, γ = 110.59 (2)°, Z = 1, V = 898.2 (4) Å^3; for 2366 data collected in the range $3 \le 2\theta \le 45°$ and 1791 data with $I > 3\sigma(I)$, R = 0.056 (R_w = 0.060). **2**: triclinic, $P\bar{1}$, a = 8.060 (3) Å, b = 10.784 (3) Å, c = 12.778 (3) Å, α = 103.40 (2)°, β = 104.15 (2)°, γ = 109.96 (2)°, Z = 1, V = 949.8 (5) Å^3; for 2497 data collected in the range $3 \le 2\theta \le 45°$ and 1885 data with $I > 3\sigma(I)$, R = 0.035 (R_w = 0.034). **3**: triclinic, $P\bar{1}$, a = 8.246 (3) Å, b = 10.805 (3) Å, c = 13.080 (4) Å, α = 68.42 (2)°, β = 96.80 (3)°, γ = 69.97 (3)°, Z = 1, V = 977.6 (6) Å^3; for 2534 data collected in the range $3 \le 2\theta \le 45°$ and 2180 data with $I > 3\sigma(I)$, R = 0.030 (R_w = 0.031).

Introduction

Linear-chain compounds of manganese(III) are rare, and those that are structurally and magnetically characterized are rarer still.[2] The single ions display complicated behavior due to a large number of excited electronic states and zero-field splittings. Optical spectroscopy is of limited use in determining the electronic origin of the zero-field splitting of the ground state, and direct measurements of D by EPR spectroscopy are usually not possible especially at X-band, since manganese(III) is an $S = 2$ non-Kramers ion and D is often greater than $h\nu$. An even-spin EPR technique has been used recently to detect resonances in $S = 2$ states of trivalent manganese complexes,[3] and the technique has been used to determine D in even-spin iron-copper exchange-coupled clusters.[4] However, magnetic susceptibility measurements have been used to provide the bulk of the information concerning the single-ion and exchange-coupled properties of these systems. As a further complication, the presence of a large single-ion anisotropy can induce anisotropy in the exchange interaction. The theory for anisotropic exchange in one-dimensional system is not well developed. Therefore, the exchange parameters in limiting cases of Heisenberg, XY, and Ising exchange must absorb the effects of this anisotropy, and this may lead to incorrect determinations of spin-Hamiltonian parameters.

Single-ion anisotropy is of considerable importance in integer-spin quasi-one-dimensional transition-metal complexes. The sign of D determines whether long-range magnetic order can occur, since long-range order is precluded by the existence of a singlet ground state. The type of magnetic order is also influenced by the symmetry relations between zero-field-split manganese(III) sublattices, and often canting phenomena are found.[5]

A further impetus for studying chain compounds of manganese(III) arises from the Haldane conjecture.[6] Haldane has theorized that, for certain values of the exchange and single-ion anisotropy, a gap opens in the excitation spectrum of antiferromagnetic integer-spin chains and the ground state is a spin singlet. Experimental evidence for a singlet ground state in $S = 1$ chains is limited, and an example of a spin-singlet ground state for an $S = 2$ chain has been announced.[7]

In this article, the electronic structure and magnetism of three manganese(III) chain compounds will be presented and discussed. These represent a series of A-B chains comprising two different manganese(III) sites alternating along the direction of the chain.

Experimental Section

Materials. Salicylic acid, sodium, potassium, and ammonium hydroxides, and methanol were purchased from Aldrich Chemical Co. $MnCl_2 \cdot 4H_2O$ was obtained from Fluka Chemical Co. All other chemicals and solvents were reagent grade. Elemental analyses were performed by Galbraith Laboratories, Knoxville, TN, or the Microanalysis Laboratory at the University of Michigan, Ann Arbor.

$(cat)_2[Mn^{III}(sal)_2(CH_3OH)_2][Mn^{III}(sal)_2] \cdot 2CH_3OH \cdot 2H_2O$ [cat = Na^+ (1), K^+ (2), NH_4^+ (3); sal = Salicylate]. All of these salts were readily prepared by the general reaction of 2 g (10 mmol) of $MnCl_2 \cdot 4H_2O$, 2.75 g of salicylic acid (20 mmol), and 20 mmol of the appropriate cation hydroxide in methanol. The solutions were stirred and aerated to oxidize the manganese salts to the +3 oxidation state. Slow evaporation of these methanol solutions resulted in pale green crystals of $Na_2[Mn^{III}(sal)_2(CH_3OH)_2][Mn^{III}(sal)_2] \cdot 2CH_3OH \cdot 2H_2O$ (**1**), $K_2[Mn^{III}(sal)_2(CH_3OH)_2][Mn^{III}(sal)_2] \cdot 2CH_3OH \cdot 2H_2O$ (**2**), and $(NH_4)_2[Mn^{III}(sal)_2(CH_3OH)_2][Mn^{III}(sal)_2] \cdot 2CH_3OH \cdot 2H_2O$ (**3**). The overall yield of **1** is 75%, of **2** is 81%, and of **3** is 69%. Anal. Calcd for **1**, $Na_2Mn_3C_{32}H_{36}O_{18}$ (mol wt 864.5): C, 44.42; H, 4.16; Mn, 12.7; Na, 5.3. Found: C, 44.90; H, 3.97; Mn, 12.88; Na, 5.16. Calcd for **2**, $K_2Mn_2C_{32}H_{36}O_{18}$ (mol wt 896.7): C, 42.85; H, 3.57; Mn, 12.27; K, 8.70. Found: C, 42.60; H, 3.69; Mn, 12.10; K, 8.56. Calcd for **3**, $C_{32}H_{44}N_2O_{18}Mn_2$ (mol wt 854.6): C, 44.93; H, 5.15; N, 3.28; Mn, 12.9. Found: C, 44.36; H, 5.44; N, 3.51; Mn, 13.01.

Collection and Reduction of X-ray Data. Suitable crystals of **1-3** were obtained as described above. These crystals were mounted in glass capillaries. Intensity data were obtained at room temperature on a Syntex $P2_1$ diffractometer using Mo Kα radiation (0.7107 Å) monochromatized from a graphite crystal whose diffraction vector was parallel to the diffraction vector of the sample. Three standard reflections were measured every 50 reflections. Modified crystal and data parameters are given in Table I. Intensity data were collected with $\theta/2\theta$ scans. The

(1) (a) The University of North Carolina. (b) The University of Michigan. (c) Aristotelian University of Thessaloniki.
(2) Hatfield, W. E.; Estes, W. E.; Marsh, W. E.; Pickens, M. W.; ter Haar, L. W.; Weller, R. W. In *Extended Linear Chain Compounds*; Miller, J. S., Ed.; Plenum Press: New York, 1982; Vol. 3, Chapter 2, p 43.
(3) Dexheimer, S. L.; Gohdes, J. W.; Chan, M. K.; Hagen, K. S.; Armstrong, W. H.; Klein, M. P. *J. Am. Chem. Soc.* **1989**, *111*, 8923.
(4) Hendrich, M. P.; Munck, E.; Fox, B. G.; Lipscomb, J. D. *J. Am. Chem. Soc.* **1990**, *112*, 5861.
(5) Kida, J.; Watanabe, T. *J. Phys. Soc. Jpn.* **1973**, *34*, 952. (b) Gregson, A. K.; Moxon, N. T. *Inorg. Chem.* **1982**, *21*, 586. (c) Kennedy, B. J.; Murray, K. S. *Inorg. Chem.* **1985**, *24*, 1552.
(6) Haldane, D. M. *Bull. Am. Phys. Soc.* **1982**, *27*, 181.
(7) Day, E. P.; Collins, T. J. *Inorganic Chemistry 91*; RACI and NZIC Conference, Hamilton, New Zealand, 1991; Abstract p 2-10. (We thank a reviewer for this information.)

0020-1669/91/1330-3900$02.50/0

Table I. Summary of Crystallographic Data for $Na_2[Mn^{III}(sal)_2(CH_3OH_2)][Mn^{III}(sal)_2]\cdot 2CH_3OH\cdot 2H_2O$ (**1**), $K_2[Mn^{III}(sal)_2(CH_3OH_2)][Mn^{III}(sal)_2]\cdot 2CH_3OH\cdot 2H_2O$ (**2**), and $(NH_4)_2[Mn^{III}(sal)_2(CH_3OH)_2][Mn^{III}(sal)_2]\cdot 2CH_3OH\cdot 2H_2O$ (**3**)

	1	**2**	**3**
formula	$Na_2Mn_2C_{32}H_{36}O_{18}$	$K_2Mn_2C_{32}H_{36}O_{18}$	$(NH_4)_2Mn_2C_{32}H_{36}O_{18}$
mol wt	864.5	896.7	854.6
a, Å	7.725 (2)	8.060 (3)	8.246 (3)
b, Å	10.596 (3)	10.784 (3)	10.805 (3)
c, Å	12.892 (3)	12.778 (3)	13.080 (4)
α, deg	102.75 (2)	103.40 (2)	68.42 (2)[a]
β, deg	104.64 (2)	104.15 (2)	96.80 (3)
γ, deg	110.59 (2)	109.96 (2)	69.97 (3)[a]
V, Å^3	898.2 (4)	949.8 (5)	977.6 (6)
cryst syst	triclinic	triclinic	triclinic
space group	$P\bar{1}$ (No. 2)	$P\bar{1}$ (No. 2)	$P\bar{1}$ (No. 2)
d_{calcd}, g/cm^3	1.598	1.572	1.452
d_{obsd}, g/cm^3	1.54	1.55	1.44
Z	1	1	1
radiation (λ, Å)	Mo Kα (0.7107)	Mo Kα (0.7107)	Mo Kα (0.7107)
abs coeff μ, cm^{-1}	7.42	8.99	6.61
temp, K	298	298	298
scan range, deg	$0 < 2\theta < 45$	$0 < 2\theta < 45$	$0 < 2\theta < 45$
no. of unique data	2366	2497	2534
no. of obsd data ($I > 3\sigma(I)$)	1791	1885	2180
R	0.056	0.035	0.030
R_w	0.060	0.034	0.031

[a] The ammonium complex **3** has been refined by using a nonstandard convention in which all angles are acute. When transformed by changing the direction of the b axis, $\alpha = 111.58°$ and $\gamma = 110.03°$.

Table II. Fractional Atomic Coordinates for $Na_2[Mn^{III}(sal)_2(CH_3OH)_2][Mn^{III}(sal)_2]$ (**1**)

atokm	x	y	z	U_{eq},[a] Å^2
Mn1	0.0 (0)	0.0 (0)	1.0 (0)	0.025
Mn2	0.5000 (0)	0.5000 (0)	1.0000 (0)	0.028
Na1	0.0132 (4)	0.3075 (3)	0.9460 (2)	0.040
O1	0.1569 (6)	−0.0400 (5)	1.1129 (4)	0.035
O2	0.1954 (6)	0.1937 (5)	1.0411 (4)	0.035
O3	0.5078 (6)	0.3482 (5)	1.0964 (4)	0.041
O4	0.2784 (6)	0.3642 (5)	0.8716 (4)	0.030
O5	0.6834 (6)	0.4583 (5)	0.9372 (4)	0.034
O6	0.7841 (7)	0.3497 (6)	0.8164 (4)	0.051
C1	0.4336 (9)	0.1960 (7)	1.2026 (6)	0.029
C2	0.3226 (9)	0.0588 (7)	1.2015 (5)	0.029
C3	0.3475 (10)	0.0201 (8)	1.2957 (6)	0.036
C4	0.5541 (11)	0.1126 (9)	1.3889 (6)	0.048
C5	0.6632 (11)	0.2490 (9)	1.3891 (6)	0.047
C6	0.6034 (10)	0.2878 (8)	1.2955 (6)	0.040
C7	0.3784 (9)	0.2475 (7)	1.1082 (6)	0.026
C8	0.2808 (10)	0.3156 (7)	0.7680 (6)	0.035
C9	0.4504 (10)	0.3136 (8)	0.7468 (6)	0.037
C10	0.4305 (12)	0.2483 (11)	0.6347 (7)	0.067
C11	0.2541 (13)	0.1919 (13)	0.5454 (7)	0.078
C12	0.0882 (12)	0.1978 (12)	0.5686 (7)	0.066
C13	0.1006 (10)	0.2563 (9)	0.6744 (6)	0.045
C14	0.6492 (10)	0.3765 (8)	0.8375 (6)	0.38
O7	0.1336 (11)	−0.0774 (7)	0.8835 (6)	0.113
C15	0.2130 (22)	−0.0165 (14)	0.8112 (12)	0.163
O8	−0.0961 (22)	0.5215 (17)	0.6799 (12)	0.220
C16	−0.2203 (33)	0.5829 (22)	0.6299 (22)	0.208
O9	−0.1217 (8)	0.3290 (6)	1.1011 (5)	0.061

[a] U_{eq} is defined as one-third of the trace of the U_{ij} tensor.

data were reduced and the model was refined by using the SHELX76 program package.[8] The structures were solved by using the SHELX86 program package. Computations were carried out on an Amdahl 5860 computer. Atomic scattering factors used were from ref 9. Hydrogen atoms were refined by using isotropic temperature factors for all structures. Unique data and final R indices are reported in Table I. Fractional atomic coordinates for **1**–**3** are given in Tables II–IV, respectively. Selected bond distances and angles for these compounds are provided in Table V.

Collection and Reduction of Magnetic Data. Magnetic susceptibility data were collected with the use of a Foner-type Princeton Applied

Table III. Fractional Atomic Coordinates for $K_2[Mn^{III}(sal)_2(CH_3OH)_2][Mn^{III}(sal)_2]$ (**2**)

atom	x	y	z	U_{eq},[a] Å^2
Mn1	0.0 (0)	0.0 (0)	1.0000 (0)	0.028
Mn2	0.5000 (0)	0.5000 (0)	1.0000 (0)	0.029
K1	−0.0066 (1)	0.3238 (1)	0.9533 (1)	0.039
O1	0.1511 (4)	−0.0356 (3)	1.1150 (2)	0.035
O2	0.1869 (4)	0.1885 (3)	1.0412 (2)	0.033
O3	0.4815 (4)	0.3437 (3)	1.0970 (3)	0.039
O4	0.2825 (3)	0.3803 (3)	0.8717 (2)	0.031
O5	0.6558 (4)	0.4389 (3)	0.9287 (2)	0.035
O6	0.7521 (4)	0.3621 (3)	0.7921 (3)	0.053
C1	0.4178 (5)	0.1925 (4)	1.2028 (3)	0.027
C2	0.3108 (5)	0.0574 (4)	1.2014 (3)	0.029
C3	0.3779 (6)	0.0157 (4)	1.2926 (4)	0.036
C4	0.5421 (6)	0.1050 (5)	1.3833 (4)	0.044
C5	0.6462 (6)	0.2406 (5)	1.3873 (4)	0.039
C6	0.5833 (6)	0.2817 (4)	1.2962 (4)	0.034
C7	0.3606(6)	0.2440 (4)	1.1086 (4)	0.030
C8	0.2737 (6)	0.3214 (4)	0.7655 (4)	0.031
C9	0.4284 (6)	0.3145 (4)	0.7365 (4)	0.034
C10	0.4010 (6)	0.2458 (5)	0.6228 (4)	0.051
C11	0.2250 (7)	0.1840 (6)	0.5365 (4)	0.054
C12	0.0737 (7)	0.1934 (5)	0.5659 (4)	0.050
C13	0.0966 (6)	0.2610 (5)	0.6767 (4)	0.037
C14	0.6217 (6)	0.3747 (4)	0.8227 (4)	0.036
O7	0.1353 (5)	−0.0756 (4)	0.8818 (3)	0.083
C15	0.2102 (10)	−0.0085 (7)	0.8121 (6)	0.109
O8	−0.1002 (6)	0.5109 (4)	0.6658 (4)	0.083
C16	−0.2045 (11)	0.5787 (8)	0.6213 (6)	0.104
O9	−0.1632 (5)	0.3187 (4)	1.1213 (4)	0.061

[a] U_{eq} is defined as one-third of the trace of the U_{ij} tensor.

Table IV. Fractional Atomic Coordinates for $(NH_4)_2[Mn^{III}(sal)_2(CH_3OH)_2][Mn^{III}(sal)_2]$ (**3**)

atom	x	y	z	U_{eq},[a] Å^2
Mn1	0.5000 (0)	0.0 (0)	0.5000 (0)	0.032
Mn2	0.0 (0)	0.5000 (0)	0.5000 (0)	0.031
N1	0.4820 (4)	0.3783 (3)	0.4514 (3)	0.044
O1	0.4755 (2)	−0.1506 (2)	0.6177 (2)	0.042
O2	0.3544 (2)	0.1476 (2)	0.5399 (2)	0.038
O3	0.1206 (2)	0.2474 (2)	0.5952 (2)	0.039
O4	0.0940 (2)	0.5111 (2)	0.3753 (1)	0.035
O5	−0.2185 (2)	0.5087 (2)	0.4218 (2)	0.038
O6	−0.4460 (3)	0.5788 (2)	0.2770 (2)	0.046
C1	0.2943 (3)	−0.0080 (3)	0.7020 (2)	0.030
C2	0.4004 (3)	−0.1416 (3)	0.7019 (2)	0.032
C3	0.4261 (4)	−0.2740 (3)	0.7921 (2)	0.040
C4	0.3524 (4)	−0.2726 (3)	0.8813 (2)	0.042
C5	0.2531 (4)	−0.1419 (4)	0.8839 (3)	0.046
C6	0.2255 (4)	−0.0121 (3)	0.7952 (2)	0.040
C7	0.2530 (3)	0.1372 (3)	0.6072 (2)	0.032
C8	0.0026 (3)	0.5576 (3)	0.2673 (2)	0.032
C9	−0.1767 (4)	0.5804 (3)	0.2333 (2)	0.035
C10	−0.2559 (4)	0.6255 (4)	0.1171 (3)	0.051
C11	−0.1635 (5)	0.6472 (4)	0.0376 (3)	0.062
C12	0.0117 (5)	0.6266 (4)	0.0710 (3)	0.060
C13	0.0948 (4)	0.5824 (3)	0.1836 (3)	0.047
C14	−0.2869 (4)	0.5560 (3)	0.3133 (2)	0.034
O7	0.2447 (3)	0.0391 (2)	0.3838 (2)	0.060
C15	0.0994 (7)	0.1756 (5)	0.3155 (5)	0.082
O8	0.2632 (4)	−0.1515 (3)	0.1596 (2)	0.066
C16	0.3173 (11)	−0.0375 (6)	0.1202 (5)	0.135
O9	0.1972 (3)	−0.1952 (2)	0.3670 (2)	0.054

[a] U_{eq} is defined as one-third of the trace of the U_{ij} tensor.

(8) Computer programs used during the structural determinations were from the SHELX program package by George Sheldrick, Institute für Anorganische Chemie der Universität Göttingen, Göttigen, Federal Republic of Germany.

(9) *International Tables for X-Ray Crystallography*; Ibers, J. A., Hamilton, W. C., Eds.; Kynoch Press: Birmingham, England, 1974; Vol. IV.

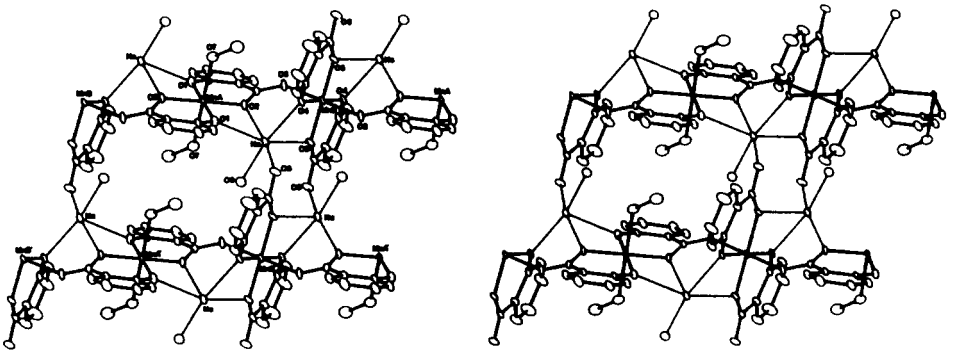

Figure 1. Stereodiagram of $Na_2[Mn^{III}(sal)_2(CH_3OH)_2][Mn^{III}(sal)_2]$ (**1**) with thermal ellipsoids at 30% probability showing two adjacent AB chains.

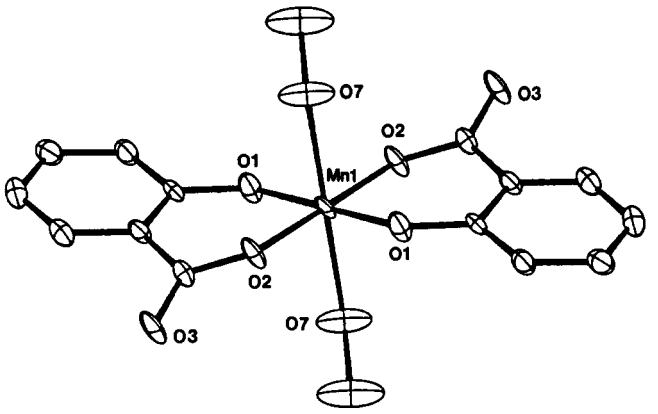

Figure 2. ORTEP diagram of the A unit of $Na_2[Mn^{III}(sal)_2(CH_3OH)_2][Mn^{III}(sal)_2]$ (**1**) with thermal ellipsoids at 30% probability.

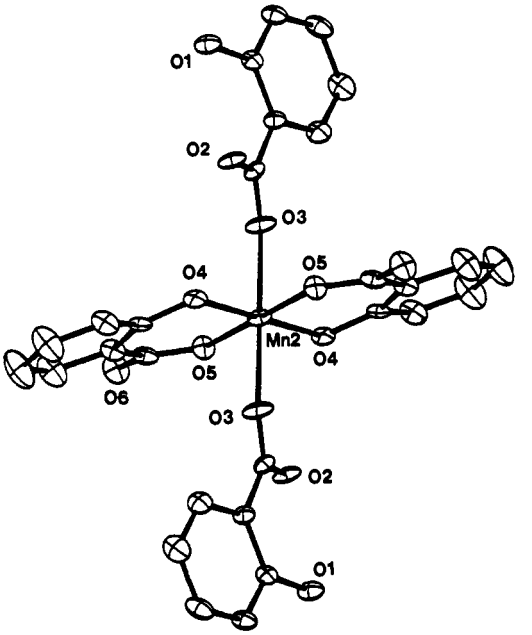

Figure 3. ORTEP diagram of the B unit of $Na_2[Mn^{III}(sal)_2(CH_3OH)_2][Mn^{III}(sal)_2]$ (**1**) with thermal ellipsoids at 30% probability.

Research Model 155 vibrating-sample magnetometer. The magnetometer was calibrated with mercury tetrathiocyanatocobaltate(II).[10] The temperature was measured with a gallium–arsenide diode which had been standardized against a calibrated diode. Diamagnetic corrections for the constituent atoms were made by using Pascal's constants.[11] Approximately 150-mg amounts of finely powdered samples were contained in precision-milled Lucite sample holders. Magnetic susceptibility and magnetization measurements were taken in applied magnetic fields ranging up to 15 kOe. A Simplex nonlinear least-squares fitting procedure[12] was used in the analysis of the experimental magnetic susceptibility data. The best fit criterion was the minimum of the function $F = \sum(\chi_i^{obsd} - \chi_i^{calcd})^2/(\chi_i^{obsd})^2$.

Results

Structural Description of AB Type Chains. The solid-state structures of three manganese(III) alternating AB type chain complexes of chemical formula $(cat)_2[Mn^{III}(sal)_2(CH_3OH)_2][Mn^{III}(sal)_2]$ have been determined. An ORTEP[13] stereodiagram of the Na^+ chain (**1**), which is isostructural with the K^+ (**2**) and NH_4^+ (**3**) salts, is provided as Figure 1. Important bond lengths and angles for **1**–**3** are provided for comparison in Table V. All three chains crystallize in the triclinic space group, $P\bar{1}$, with both Mn1 and Mn2 located on crystallographic inversion centers. The resultant molecular structure is composed of three parts: (i) the polyhedron of Mn1 in $Mn^{III}(sal)_2(CH_3OH)_2$ (the A unit), (ii) the polyhedron of Mn2 in $Mn^{III}(sal)_2$ (the B unit), which is bridged to the A structure by two carboxylates, and (iii) the monovalent cation coordination environment.

The Mn1 Polyhedron (A Unit). As illustrated in Figure 2, this Mn(III) ion is six-coordinate by virtue of two bidentate salicylate ligands that form a tetragonal plane and two axial solvent methanols. The in-plane carboxylate and phenolate oxygens are at relatively short average distances of 1.925 (±0.001) Å and 1.873 (±0.003) Å, respectively, with little variation across the three structures. In contrast, the coordinated methanol oxygens reside at longer distances [≤2.23 (±0.03) Å]. Such marked axial elongations are typical for high-spin d^4 systems. As may be seen in Table V, the Mn1–O7 bond is the most sensitive to cation substitution, changing as much as 0.057 Å and following the order $Na^+ < K^+ < NH_4^+$. This observation provides information about the microscopic orientation of electron density in the unit and, as discussed more fully below, is consistent with an energy diagram which places the unoccupied $d_{x^2-y^2}$ orbital at highest energy.

Despite the axial elongation, all of the O–Mn–O bond angles are within 5° of the predicted octahedral value. The O2–C7–C1–C2–O1 chelate structure is nearly planar. The O2–C7–O3 angle for the bridging carboxylate (121.8°) undergoes a slight expansion compared to the nonbridging carboxylate (119.4°) in the B unit.

The Mn2 Polyhedron (B Unit). This Mn(III) ion is also six-coordinate with four of its sites filled with salicylate oxygen atoms (O4, O5, O4B, O5B), as shown in Figure 3. However, the axial ligands of this metal are carboxylate oxygens (O3 and O3B) from the salicylates of the A unit. This leads to the anti–syn AB type alternating chains of Figure 1. Once again, the two bidentate salicylate groups form the basis for the *xy* plane with short Mn–O distances that are indistinguishable from those of the A unit and are relatively insensitive to cation substitution [Mn2–O4 = 1.872 (±0.005) Å; Mn2–O5, 1.922 (±0.006) Å]. The axial carboxylates of Mn2 show even greater tendency to elongate than the methanol

(10) Brown, D. B.; Crawford, V. H.; Hall, J. W.; Hatfield, W. E. *J. Phys. Chem.* **1977**, *81*, 1303.
(11) (a) Figgis, B. N.; Lewis, J. In *Modern Coordination Chemistry*; Lewis, J., Wilkins, R. G., Eds.; Interscience: New York, 1960; Chapter 6, p 403. (b) Kŏnig, E. *Magnetic Properties of Transition Metal Compounds*; Springer-Verlag: West Berlin, 1966. (c) Weller, R. R.; Hatfield, W. E. *J. Chem. Educ.* **1979**, *56*, 652.
(12) Nelder, J. A.; Mead, R. *Comput. J.* **1965**, *7*, 308.
(13) Johnson, C. K. ORTEP-II: A FORTRAN Thermal-Ellipsoid Plot Program for Crystal Structure Illustrations. Report ORNL-5138; Oak Ridge National Laboratory: Oak Ridge, TN, 1976.

Table V. Selected Bond Distances and Angles for $Na_2[Mn^{III}(sal)_2(CH_3OH_2)][Mn^{III}(sal)_2]\cdot 2CH_3OH\cdot 2H_2O$ (**1**), $K_2[Mn^{III}(sal)_2(CH_3OH_2)][Mn^{III}(sal)_2]\cdot 2CH_3OH\cdot 2H_2O$ (**2**), and $(NH_4)_2[Mn^{III}(sal)_2(CH_3OH_2)][Mn^{III}(sal)_2]\cdot 2CH_3OH\cdot 2H_2O$ (**3**)[a]

	bond distances, Å					
	1	**2**	**3**[b]	Δ_{1-2}	Δ_{2-3}	Δ_{1-3}
Mn1–cat	3.452 (3)	3.692 (1)	3.845 (2)	−0.240	−0.153	0.393
Mn2–cat	3.383 (2)	3.691 (1)	3.944 (2)	−0.309	0.253	−0.562
Mn1–Mn2	5.347 (3)	5.520 (2)	5.561 (3)	−0.173	−0.041	−0.214
Mn1–O1	1.873 (4)	1.870 (3)	1.875 (2)	0.003	−0.005	−0.002
Mn1–O2	1.926 (4)	1.925 (2)	1.925 (2)	0.001	0	0.001
Mn1–O7	2.197 (6)	2.231 (3)	2.254 (2)	−0.034	−0.023	−0.057
Mn2–O4	1.877 (4)	1.870 (3)	1.869 (2)	0.007	0.001	0.008
Mn2–O5	1.928 (4)	1.920 (3)	1.918 (2)	0.008	0.002	0.010
Mn2–O3	2.247 (4)	2.300 (3)	2.310 (2)	−0.053	−0.010	−0.063
cat–O6*	2.349 (6)	2.680 (3)	**2.796 (2)**	−0.331	−0.116	−0.447
cat–O9	2.476 (6)	2.746 (4)	**2.833 (2)**	−0.270	−0.087	−0.357
cat–O1′	2.513 (6)	2.748 (4)	**2.848 (2)**	−0.235	−0.100	−0.335
cat–O2	2.432 (5)	2.698 (3)	**2.936 (2)**	−0.266	−0.238	−0.504
cat–O4	2.421 (5)	2.720 (3)	**2.887 (2)**	−0.299	−0.167	−0.466
cat–O5′	2.530 (6)	2.829 (4)	**3.079 (3)**	−0.299	−0.250	−0.549
	bond angles, deg					
	1	**2**	**3**	Δ_{1-2}	Δ_{2-3}	Δ_{1-3}
O1′–Mn1–O2	93.9 (2)	92.6 (1)	92.7 (1)	1.3	−0.1	1.2
O1′–Mn1–O7	88.3 (2)	88.6 (1)	89.5 (1)	−0.3	−0.9	−1.2
O2–Mn1–O7	90.3 (2)	88.9 (1)	87.5 (1)	1.4	1.4	2.8
O3–Mn2–O4	95.6 (2)	96.2 (1)	96.7 (1)	−0.6	−0.5	−1.1
O3–Mn2–O5	90.0 (2)	91.2 (1)	91.9 (1)	−1.2	−0.7	−1.9
O4–Mn2–O5	92.8 (2)	91.7 (1)	92.0 (1)	1.1	−0.3	0.8
O2–cat–O4	81.7 (2)	77.0 (1)	71.5 (1)	4.7	5.5	10.2
O2–cat–O6*	163.4 (2)	156.3 (1)	152.8 (1)	7.1	3.5	10.6
O2–cat–O9	87.8 (2)	88.5 (1)	88.2 (1)	−0.7	0.3	−0.4
O2–cat–O1′	63.4 (2)	57.6 (1)	53.9 (1)	5.8	3.7	9.5
O2–cat–O5	86.4 (2)	83.2 (1)	76.7 (1)	3.2	6.5	9.7
O4–cat–O6*	99.6 (2)	97.8 (1)	99.9 (1)	1.8	−2.1	−0.3
O4–cat–O9	153.3 (2)	155.0 (1)	149.0 (1)	−1.7	6.0	4.3
O4–cat–O1′	107.0 (2)	100.9 (1)	95.3 (1)	6.1	5.6	11.7
O4–cat–O5′	64.0 (2)	56.7 (1)	52.2 (1)	7.3	4.5	11.8
O6*–cat–O9	97.4 (2)	103.3 (1)	108.2 (1)	−5.9	−4.9	−10.8
O6*–cat–O1′	100.7 (2)	101.9 (1)	103.0 (1)	−1.2	−1.1	−2.3
O6*–cat–O5′	109.1 (2)	113.5 (1)	119.2 (1)	−4.4	−5.7	−10.1
O9–cat–O1′	89.8 (2)	87.9 91)	90.9 (1)	1.9	−3.0	−1.1
O9–cat–O5′	91.0 (2)	101.8 (1)	101.2 (1)	−10.8	0.6	−10.2
O1′–cat–O5′	149.7 (2)	139.5 (2)	128.8 (1)	10.2	10.8	20.9
Mn1–O1′–cat	103.2 (2)	104.5 (1)	107.2 (1)	−1.3	−2.7	−4.0
Mn1–O2–cat	104.2 (2)	104.7 (1)	102.5 (1)	−0.5	2.2	1.7
Mn2–O4–cat	103.1 (2)	105.6 (1)	110.2 (1)	−2.5	−4.6	−7.1
Mn2–O5′–cat	97.8 (2)	100.3 (1)	101.7 (1)	−2.5	−1.4	−3.9
Mn1–O2–C7	126.0 (4)	128.0 (3)	128.7 (2)	−2.0	−0.7	−2.7
O2–C7–O3	120.2 (6)	120.7 (4)	121.1 (2)	−0.5	−0.4	−0.9
Mn2–O3–C7	134.3 (4)	139.8 (3)	140.3 (2)	−5.5	−0.5	−6.0
	dihedral angles, deg					
	1	**2**	**3**	Δ_{1-2}	Δ_{2-3}	Δ_{1-3}
O1–O2–O1B–O2B/ O4–O5–O4B–O5B	84.4	82.9	85.0	1.5	−2.1	−0.6

[a] Oxygens with asterisks denote atoms from adjacent chain (chain 2). Primed atoms are symmetry-related first-coordination-sphere oxygen atoms. [b] Bold separations are contacts associated with weak hydrogen bonds.

molecules on Mn1, with a range of values of 0.063 Å. Furthermore, the average [2.29 (±0.04) Å] and individual Mn2–O3 distances are consistently longer than Mn1–O7 for the respective salts, although the same trend in axial bond length elongation is observed. This suggests that the lowest energy d_{z^2} orbital in all of these complexes resides on Mn2 in **3**.

The ramifications for chain structure associated with cation substitution are most apparent in the B unit. Greater deviations from octahedral bond angles are observed in the B unit, with the O3–Mn2–O4 angle as large as 96.7 (1)°. The O3–Mn2–O4 angle in particular reflects the tilting of the B unit *xy* plane with respect to the *xy* plane of the A unit. The result of this tilting is compared for **1** and **3** in Figure 4. The two chains have been oriented such that the central bridging carboxylates (O2–C7–O3) are placed on top of one another. Notice that the A units closest to this carboxylate have nuclear coordinates that are almost superimposable. In contrast, a marked tilting of the B unit tetragonal plane of **3** (solid line) is seen relative to **1** (dashed line). The

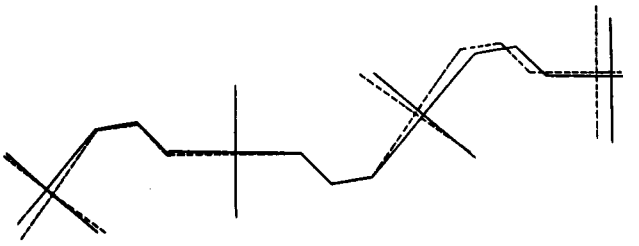

Figure 4. Line diagram illustrating the elongation of the AB chain structure associated with cation substitution. The dashed line is the trace of **1**, while the solid line is the trace of **3**. The diagram was generated by overlapping the O2–C7–O3 atoms of the two structures.

greater Jahn–Teller distortion of the ammonium versus sodium forms also leads to a larger Mn–Mn separation. The result of more obtuse angles and longer Mn–O distances for the ammonium B unit relative to the sodium form is that the NH_4^+ chain is a

more elongated structure. This is clearly demonstrated by comparing the (n + 1) A units of the **1** and **3** chains, where there is a marked shift of the solid and dashed lines in Figure 4.

Cation Polyhedra. Charge balance is achieved by the incorporation of two monovalent cations which are associated with each AB unit. As would be expected for systematic cation substitution, the greatest modifications in structure of these AB chains are in the channels surrounding the monovalent cation. Once again, absolute distances, angles, and deviations between structures are presented in Table V. The two alkali-metal cations are six-coordinate, shown for the Na^+ cation in Figure 1, having contacts with six oxygen atoms from two chains. The average Na^+–O and K^+–O distances, 2.453 and 2.737 Å, respectively, are very close to the values predicted by Shannon[14] for these bonds (Na^+, 2.40 Å; K^+, 2.76 Å), indicating that the observed distortions are primarily a result of cation size. A better description for the ammonium cation is that it forms single hydrogen bonds to solvent or carboxylate oxygens not bound to manganese [O6(carboxylate)/chain 2 and O9(lattice water)] and bifurcated hydrogen bonds across the edges of the A and B tetragonal planes [O1′(phenolate) and O2(carboxylate)/chain 2, O4(phenolate) and O5′(carboxylate)/chain 1]. The carboxylate oxygens participating in the bifurcated hydrogen bonds are more weakly associated than the phenolate oxygen atoms. This fact is reflected in the corresponding cation–oxygen separations [2.936 (2) and 3.079 (3) Å] which are 0.1–0.2 Å longer than observed for the remaining nitrogen–oxygen contacts (N–O_{av} = 2.834 Å).

As commented upon above, it is the B unit which suffers the greatest distortion upon cation substitution. This is reflected in the greater spread in Mn2–cat (0.562 Å) versus Mn1–cat (0.393 Å) distances and also the larger angular dependence (e.g.: Mn–O1′–cat, Δ_{1-3} = 4°; Mn2–O4–cat, Δ_{1-3} = 7.1°). In general, the ranges in Mn1–Mn2 separation and angular perturbations from **1** to **3** are ≈4%, while alterations of Mn–cat distances and angles are as large as 17%.

Analysis of the Magnetic Susceptibility Data. The magnetic behavior of d^4 high-spin Mn(III) ions in a magnetic field is quite complex, being complicated by exchange interactions, low-symmetry ligand fields, g-tensor anisotropy, and the fact that d^4 ions are Jahn–Teller active. In order to account for all of these factors, the following spin-Hamiltonian is appropriate for the case of a linear array of exchange-coupled Mn(III) ions:

$$\mathbf{H} = g_{\parallel}\beta\sum_{i=1}^{N}(H_z \cdot S_{iz}) + g_{\perp}\beta\sum_{i=1}^{N}(H_x \cdot S_{ix} + H_y \cdot S_{iy}) - 2J\sum_{i=1}^{N}(S_i \cdot S_{i+1}) + D\sum_{i=1}^{N}[S_{iz}^2 - \tfrac{1}{3}S(S+1)] + E\sum_{i=1}^{N}(S_{ix}^2 + S_{iy}^2)$$

For the A–B chains, application of this Hamiltonian becomes quite difficult due to the large number of parameters. Since the two sites are subjected to different coordination environments, there must be a separate D, E, $g_{\parallel}$, and $g_{\perp}$ for each ion. The analysis of these chains can be simplified by assuming an idealized point symmetry. The analysis of the crystal structure indicates that both the Mn1 and Mn2 sites along the chain are of approximate D_{4h} symmetry. This treatment is valid, since it has been shown that the dependence of the magnetic susceptibility on the rhombic splitting parameter E is negligible. To a first approximation, the parameters $g_{\parallel}$, $g_{\perp}$, and D will be considered the same for the Mn1 and Mn2 sites. This reduces the number of parameters to a manageable size.

Magnetic Susceptibility of $K_2[Mn^{III}(sal)_2(CH_3OH)_2][Mn^{III}(sal)_2]$. The powder average molar magnetic susceptibility in an applied field of 10 kOe is shown in Figure 5. Magnetic susceptibility data collected in an applied magnetic field of 5 kOe are given in Figure S1 (supplementary material). A maximum in the susceptibility is not observed down to 1.9 K. The effective magnetic moment at 70 K is 4.7 μ_B in a magnetic field of 10 kOe and 4.8 μ_B in a field of 5 kOe. These values are in accord with the spin-only magnetic moment for a high-spin d^4 ion. A severe

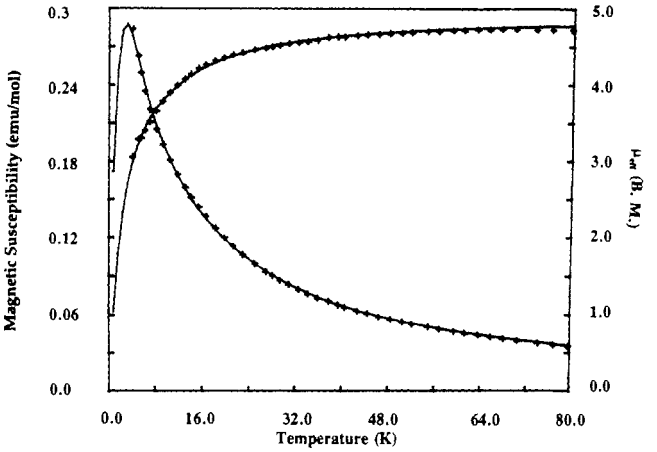

Figure 5. Magnetic susceptibility and magnetic moment of $K_2[Mn^{III}(sal)_2(CH_3OH)_2][Mn^{III}(sal)_2]$ in an applied magnetic field of 10 kOe. The solid lines were generated by the best fit parameters given in the text.

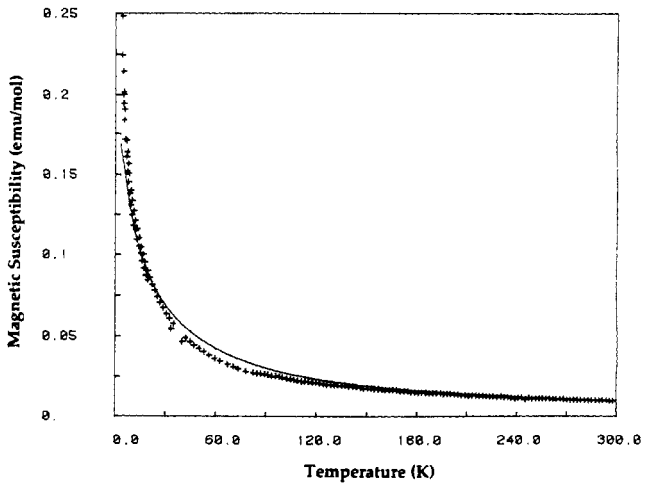

Figure 6. Magnetic susceptibility of $Na_2[Mn^{III}(sal)_2(CH_3OH)_2][Mn^{III}(sal)_2]$ at an applied field strength of 1 kOe. The solid line was generated by the model and the best fit parameters given in the text.

reduction in magnetic moment begins below 30 K, as shown in Figure S1. This reduction is due to large single-ion zero-field-splitting effects with the possibility of an exchange interaction playing a minor role.

For the analysis of the data of $K_2[Mn^{III}(sal)_2(CH_3OH)_2][Mn^{III}(sal)_2]$, a model was constructed along the lines of Marathe and Mitra[15] by assuming the magnetic susceptibility may be expressed as a combination of single-ion and exchange terms. In their model, the $Ng^2\mu_B^2S(S+1)/3kT$ term in the expression derived by Fisher[16] for the isotropic Heisenberg nearest-neighbor chain was replaced by χ_{ZFS}, which was calculated by using the Hamiltonian

$$\mathcal{H} = g_{\parallel}\mu_B H_z \cdot S_z + g_{\perp}\mu_B(H_x \cdot S_x + H_y \cdot S_y) + D[S_z^2 + \tfrac{1}{3}S(S+1)]$$

It was found in this work that the polynomial expression of Hall[17] gives better fits to the data, and it was used to replace the [(1 + U)/(1 − U)] term in the expression given by Marathe and Mitra.[15] The final expression is

$$\chi_{chain} = \chi_{ZFS}\frac{A + Bx^2}{1 + Cx + Dx^3}$$

This model yielded the values $g_{\parallel}$ = 1.995, $g_{\perp}$ = 1.995, J = −0.23 cm^{-1}, and D = −9 cm^{-1}. The 10 kOe data set was used in the fitting calculations. The magnetic susceptibility calculated by

(14) Shannon, R. D. *Acta Crystallogr.* **1976**, *A32*, 751.

(15) Marathe, V. R.; Mitra, S. *J. Chem. Phys.* **1983**, *78*, 915.
(16) Fisher, M. E. *Am. J. Phys.* **1964**, *32*, 343.

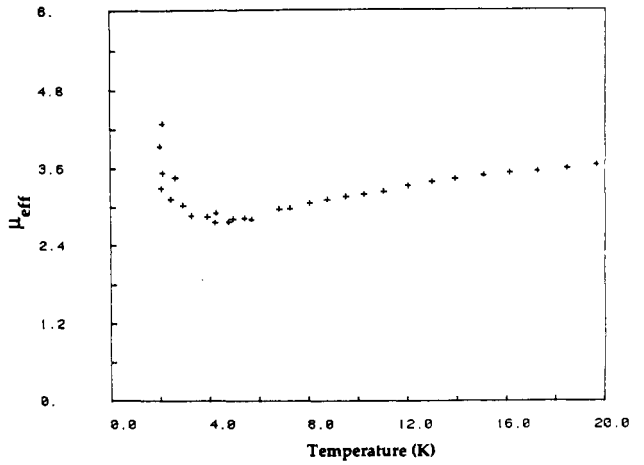

Figure 7. Effective magnetic moment data for $Na_2[Mn^{III}(sal)_2(CH_3OH)_2][Mn^{III}(sal)_2]$ showing the onset of weak ferromagnetism.

using the best fit parameters is shown as the solid line in Figure 5.

Magnetic Susceptibility of $Na_2[Mn^{III}(sal)_2(CH_3OH)_2][Mn^{III}(sal)_2]$. The temperature-dependent magnetic susceptibility of $Na_2[Mn^{III}(sal)_2(CH_3OH)_2][Mn^{III}(sal)_2]$ in a magnetic field of 1 kOe is shown in Figures 6 and 7. Upon close inspection of the data in Figure 7, a magnetic phase transition is apparent with an onset temperature of 4.0 K. Since the susceptibility does not turn over at the lowest temperatures studied, it is assumed that the intrachain interactions are small in $Na_2[Mn^{III}(sal)_2(CH_3OH)_2][Mn^{III}(sal)_2]$ and the system may be treated by the hybrid model proposed by Marathe and Mitra,[15] as modified in this work. A molecular field term was added in order to describe the interchain interactions that are expected in this chain. The expression for the magnetic susceptibility becomes

$$\chi_M^{mf} = \chi_M/(1 - 2zJ'\chi_M/Ng^2\mu_B^2)$$

The best fit parameters obtained are $J = -0.23$ cm^{-1}, $D = -20.3$, and $zJ' = -0.81$ cm^{-1}, with the values for $g_\parallel$ and $g_\perp$ being held constant at 2.00. The best fit is shown in Figure 6. The minimum temperature used in the fitting process was 7 K in order to eliminate the possibility of pretransitional effects influencing the spin-Hamiltonian parameters. The fact that zJ' is larger than the intrachain coupling constant is reflective of the impending onset of three-dimensional ordering. As in the case of $K_2[Mn^{III}(sal)_2(CH_3OH)_2][Mn^{III}(sal)_2]$, the zero-field splitting is extremely large and is of questionable validity in this case, since D values of this magnitude are rarely seen and D may reflect long-range ordering. However, a nonnegligible intrachain interaction is evident and, as will be shown below, plays an important role in the origin of the observed weak ferromagnetism.

Magnetic Susceptibility of $(NH_4)_2[Mn^{III}(sal)_2(CH_3OH)_2][Mn^{III}(sal)_2]$. The magnetic susceptibility of $(NH_4)_2[Mn^{III}(sal)_2(CH_3OH)_2][Mn^{III}(sal)_2]$ was determined in a magnetic field of 10 kOe and is shown in Figure 8. An apparent rounding in the susceptibility around 8 K coupled with a temperature-dependent magnetic moment signifies that the exchange interactions in this compound are greater that in the alkali metal cation counterparts. The upturn in the susceptibility below 8 K is probably due to a paramagnetic impurity. The polynomial expression of Hall[17] was used in the analysis of the data, and the best fit to the data in the temperature range 2–46 K yielded $g = 2.09$, $D = -7.0$ cm^{-1}, and $J = -0.70$ cm^{-1} with an impurity correction of 7%. The best fits are shown as the solid lines in Figure 8.

Isothermal Magnetization Measurements. Isothermal magnetization data as a function of magnetic field strength were obtained for fields between 50 Oe and 15 kOe at 2.66 and 4.17 K for

(17) Hall, J. W. Ph.D. Dissertation, The University of North Carolina, Chapel Hill, NC, 1977.

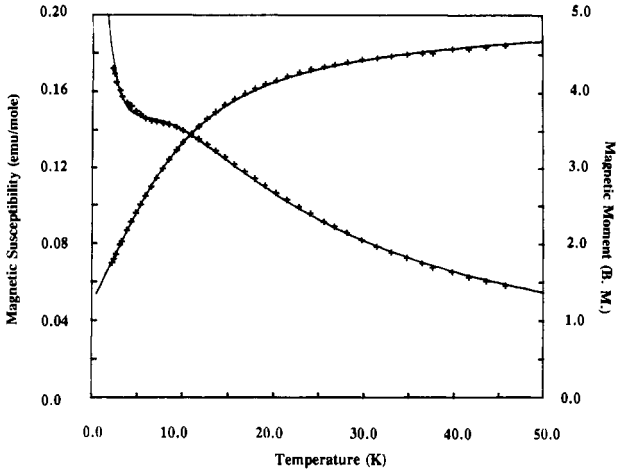

Figure 8. Magnetic susceptibility $(NH_4)_2[Mn^{III}(sal)_2(CH_3OH)_2][Mn^{III}(sal)_2]$ at an applied field strength of 10 kOe. The solid line was generated by the model and the best fit parameters given in the text.

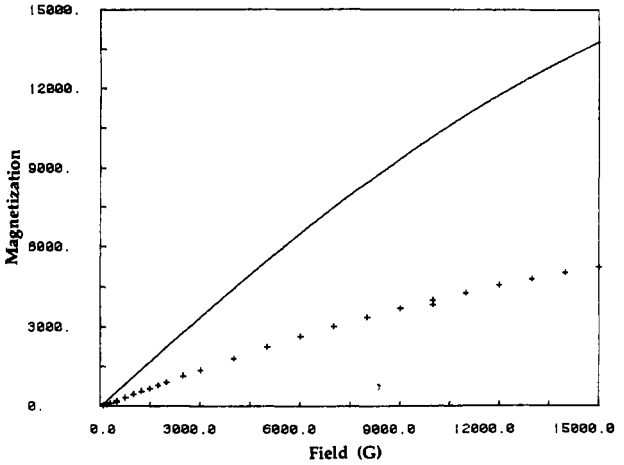

Figure 9. Magnetization vs applied field for $K_2[Mn^{III}(sal)_2(CH_3OH)_2][Mn^{III}(sal)_2]$ at 2.66 K. The solid line is the Brillouin function for $S = 2$.

$K_2[Mn^{III}(sal)_2(CH_3OH)_2][Mn^{III}(sal)_2]$, and the data are shown in Figures 9 and S2 (supplementary material). The observed magnetization is significantly reduced from that expected for an $S = 2$ paramagnet at both temperatures studied. The magnetization data at 2.66 K start to saturate at approximately 6 kOe. This is in the same field range that saturation should occur for an $S = 2$ paramagnet. The solid lines drawn were calculated from the Brillion function for $S = 2$

$$B_j(x) = \frac{2J+1}{2J}\coth\left(\frac{(2J+1)x}{2J}\right) - \frac{1}{2J}\coth\left(\frac{x}{2J}\right)$$

with $g_{av} = 2.00$. In this equation, J is the angular momentum quantum number and $x = Jg\mu_BH/kT$. The observed reduction in magnetization at the two temperatures studied is consistent with the exchange coupling determined for this compound.

Magnetization measurements as a function of applied field for $Na_2[Mn^{III}(sal)_2(CH_3OH)_2][Mn^{III}(sal)_2]$ were made at 2.16 K. The data are shown in Figure 10. The observed tendency toward saturation at relatively low fields is in accord with the weak ferromagnetism evident in the susceptibility measurements. These data are consistent with the onset of three-dimensional long-range antiferromagnetic order, which results in an uncompensated spin arrangement in the ordered state.

Discussion

Molecular Orbital Description of the Exchange Pathways. As discussed previously, the structural perturbations in this system are provided solely by the cation. The ramifications for exchange coupling seem at first glance to be negligible, since there are only

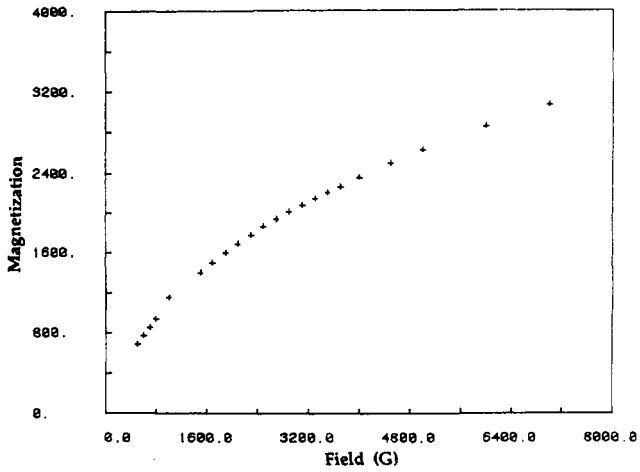

Figure 10. Magnetization vs applied field for $Na_2[Mn^{III}(sal)_2(CH_3OH)_2][Mn^{III}(sal)_2]$ at 2.16 K showing the effect of weak ferromagnetism.

subtle structural changes upon cation substitution. The observed axial elongation and idealized D_{4h} site symmetry place the unpaired electron in an orbital of a_{1g} symmetry (the d_{z^2} orbital). An exchange pathway exists via the O2–C7–O3 carboxylate group of the salicylate ligand bound to Mn1. However, superexchange would proceed formally between the $d_{x^2-y^2}$ type orbital and a d_{z^2} orbital. Even smaller deviations from idealized D_{4h} site symmetry result in a molecular orbital of the form $\Phi = c_1\Phi_1 + c_2\Phi_2$, where Φ_1 is a d_{z^2} orbital and Φ_2 is a $d_{x^2-y^2}$ orbital. Therefore, the lowering of the molecular point symmetry allows for the possibility of weak antiferromagnetic interactions between Mn1 and Mn2 subunits along the chain.

In the case of the $(NH_4)_2[Mn^{III}(sal)_2(CH_3OH)_2][Mn^{III}(sal)_2]$ chain, a second exchange pathway is possible as a result of hydrogen bonding. Unpaired electron density from the Mn2 d_{z^2} orbital is delocalized onto the carboxylate (O2–C7–O3) of one of the Mn1 salicylate ligands. There is a hydrogen bond between the ammonium ion and the carboxylate oxygen atom (O5) as well as one between the ammonium ion and the lattice water oxygen (O9). Finally, there is a hydrogen bond between the water molecule and the methanolic oxygen (O7) in the axial position on Mn1. This pathway would lead to an antiferromagnetic superexchange interaction involving both magnetic d_{z^2} orbitals on neighboring manganese sites along the chain. The shorter Mn(B)–O3 bond distance in $Na_2[Mn^{III}(sal)_2(CH_3OH)_2][Mn^{III}(sal)_2]$ and the second orbital exchange pathway via hydrogen bonding in $(NH_4)_2[Mn^{III}(sal)_2(CH_3OH)_2][Mn^{III}(sal)_2]$ may explain the weak exchange coupling constants observed in these compounds.

A consistent picture is beginning to emerge that describes the effect of cation substitution on the magnetic properties of these chains in general and their spin dimensionality in particular. The spatial arrangement of the A–B chain segment ensures intrachain interactions will be minimized, since the exchange interaction proceeds formally between the nonmagnetic $d_{x^2-y^2}$ orbital on the A unit and the magnetic d_{z^2} orbital on the B unit. Intrachain exchange coupling should be sensitive to the Mn2–O3 bond distance, since this is the pathway for through-bond spin exchange between manganese sites along the chain. The Jahn–Teller-active Mn(III) sites are not chemically equivalent, and their respective Jahn–Teller axes are not collinear. This results in complications in the modeling of the experimental data and the potential for weak ferromagnetism upon the onset of long-range antiferromagnetic order in $Na_2[Mn^{III}(sal)_2(CH_3OH)_2][Mn^{III}(sal)_2]$ due to the close spacing of the chains as a result of the small sodium cation.

The linear chain $K_2[Mn^{III}(sal)_2(CH_3OH)_2][Mn^{III}(sal)_2]$ behaves magnetically as an antiferromagnetically exchange-coupled one-dimensional system. The combination of high site symmetry about Mn1 and the Mn2–O3 bond distance of 2.300 (3) Å results in the relatively small intrachain coupling constant. The explanation for the zero-field splitting of -9 cm^{-1} requires further discussion. From second-order perturbation theory, an expression for the zero-field-splitting parameter can be derived in terms of the one-electron spin–orbit coupling constant ζ and the energy differences between the ground-state electronic configuration $^5B_{1g}$ and the excited $^5E_g(\Delta E_1)$, $^5B_{2g}(\Delta E_2)$, and $^3E(\Delta E_3)$ states:[18]

$$D = \frac{1}{16}\zeta^2\left(\frac{1}{\Delta E_1} - \frac{4}{\Delta E_2} - \frac{4}{\Delta E_3}\right)$$

From this expression, it can easily be seen why D is negative in Mn(III) complexes with effective D_{4h} site symmetry, since the two negative contributions to D are weighted 4 times more heavily than the positive contribution. Large negative values for D may result from significant mixing of the ^3E excited state, which originates from the $^3T_1$ state in O_h symmetry. The Tanabe–Sugano diagram[19] for the high-spin d^4 configuration in an octahedral field shows that the $^3T_1$ excited state can closely approach the ground state in energy for values of Dq/B greater than 2.

As expected from its structural similarity to the potassium salt, the magnetic data for $Na_2[Mn^{III}(sal)_2(CH_3OH)_2][Mn^{III}(sal)_2]$ provide direct evidence for a higher spin dimensionality. Although the intrachain exchange is also small (-0.29 cm^{-1}), exchange-coupling constants of this magnitude have pronounced effects on the magnetic properties of higher spin low-dimensional materials in the low-temperature range. Since long-range antiferromagnetic order begins at 4 K, the fitting was accomplished at temperatures higher than this to avoid the complications brought about by pretransitional effects. As in the case of $K_2[Mn^{III}(sal)_2(CH_3OH)_2][Mn^{III}(sal)_2]$, the zero-field-splitting parameter is quite large, possibly indicative of a high degree of mixing between the ^3E_g excited state and the ground state. It was found that a mean-field term needed to be added to the Hamiltonian in order to obtain a good fit to the data. The large value of $zJ' = -0.8$ cm^{-1} has its origins in any anisotropic intrachain exchange and interchain interaction. Both of these factors seem to be possible contributors in light of the large single-ion anisotropy and the shortened interchain contacts brought about by the smaller ionic radius of the sodium cation. In light of the crystal structure, the observation of weak ferromagnetism in $Na_2[Mn^{III}(sal)_2(CH_3OH)_2][Mn^{III}(sal)_2]$ is most likely due to a canting of the sublattice magnetizations with respect to each other.

There are two mechanisms by which weak ferromagnetism may occur. These are the single-ion anisotropy (commonly referred to as g-tensor anisotropy in systems that may be described by a fictitious $S = {}^1/_2$ spin-Hamiltonian, since there is no single-ion anisotropy in this basis) and antisymmetric spin–spin coupling. If any two individual single-ion anisotropy energies are such that the condition $E_i = E_j$ is met, canting between the two sublattice magnetizations cannot occur. This is due to the fact that the two spins are collinear, and antiferromagnetic ordering should occur along this direction. However, if $E_i \neq E_j$, the easy axes of the two sublattices are not collinear and weak ferromagnetism may result.

The second canting mechanism involves the addition of an extra term in the spin-Hamiltonian which takes the form

$$\mathbf{H} = \mathbf{D}_{ij}\cdot(S_i \times S_j)$$

where $\mathbf{D}_{ij}$ is a constant vector. This Hamiltonian describes antisymmetric exchange, the Dzyaloshinski–Moriya interaction.[20-22] The symmetry aspects of this interaction are such that if a symmetry element of a given space group transforms different sublattice magnetization vectors into each other, weak ferromagnetism cannot occur in zero field. The energy of the spin system under this Hamiltonian is proportional to the cross product $S_i \times S_j$. Since $S_i \times S_j = s_1 s_2(\sin\theta)\mathbf{1}$, where **1** is a unit vector perpendicular to the plane formed by the S_i and S_j vectors, the minimum in system

(18) Dugad, L. B.; Behere, D. V.; Marathe, V. R.; Mitra, S. *Chem. Phys. Lett.* **1984**, *104*, 353.
(19) Tanabe, Y.; Sugano, S. *J. Phys. Soc. Jpn.* **1954**, *9*, 753, 766.
(20) Dzyaloshinski, I. *J. Phys. Chem. Solids* **1958**, *4*, 241.
(21) Moriya, T. *Phys. Rev.* **1960**, *117*, 635.
(22) Moriya, T. *Phys. Rev.* **1960**, *120*, 91.

energy is obtained when $\theta = \pi/2$ and the sublattice magnetizations are perpendicular to one another. The magnitude of the vector D_i is approximately equal to $[(g - 2)/2]\cdot J$, and the canting is maximized when there exists a large g tensor anisotropy in the presence of large intrachain exchange coupling.

Expressions for the parallel and perpendicular g values of manganese(III) in a tetragonal field may be derived from perturbation theory:

$$g_{\parallel} = 2 - 2\zeta(1/\Delta_1) \qquad g_{\perp} = 2 - \tfrac{1}{2}\zeta(1/\Delta_2)$$

Clearly the g values in moderate to strong ligand fields are nearly isotropic. Since the intrachain exchange coupling is very weak, the contribution from the antisymmetric Dzyaloshinski-Moriya interaction is negligible. As discussed previously, the space group of $Na_2[Mn^{III}(sal)_2(CH_3OH)_2][Mn^{III}(sal)_2]$ is $P\bar{1}$. The manganese sites A and B that make up the unit cell lie on inversion centers, and their Jahn-Teller axes are not collinear. The two sublattices are not chemically equivalent, so there can be no symmetry element that transforms the two sublattice magnetizations into one another. Therefore, the single-ion anisotropy is the dominant contribution to the observed weak ferromagnetism, and in the ordered state $Na_2[Mn^{III}(sal)_2(CH_3OH)_2][Mn^{III}(sal)_2]$ may be tentatively classified as a two-sublattice canted antiferromagnet.

It is interesting to note that the linear-chain compound $(NH_4)_2MnF_5$, which comprises canted, Jahn-Teller-distorted MnF_6^{3-} octahedra, also displays weak ferromagnetism.[3] The relative tilting of the respective octahedra is much less than that observed in $Na_2[Mn^{III}(sal)_2(CH_3OH)_2][Mn^{III}(sal)_2]$, and the intrachain exchange coupling is approximately 30 times larger. Single-crystal magnetic susceptibility measurements determined the canting was due to the single-ion anisotropy, and the canting angle between spins along the chain axis was determined to be 0.83°.

The third linear chain in the A-B series, $(NH_4)_2[Mn^{III}(sal)_2(CH_3OH)_2][Mn^{III}(sal)_2]$ behaves as a one-dimensional Heisenberg antiferromagnet. Unfortunately, the low-temperature behavior is complicated by chain-end effects caused by grinding the sample prior to packing the VSM sample holder, a magnetic impurity, or both. The experimentally determined value of -0.7 cm^{-1} for the intrachain exchange is 3 times larger than that of the sodium salt, but the Mn-Mn separation increases by 0.041 Å and the Mn2-O3 bond distance is 0.063 Å longer. This is consistent with the previous arguments put forth concerning the intrachain exchange in $Na_2[Mn^{III}(sal)_2(CH_3OH)_2][Mn^{III}(sal)_2]$ and the corresponding K^+ salt. Obviously, an additional exchange pathway must be operative. Since the only major structural change between $(NH_4)_2[Mn^{III}(sal)_2(CH_3OH)_2][Mn^{III}(sal)_2]$ and the sodium and potassium salts is the incorporation of a cation capable of hydrogen bonding, the ammonium cation must be involved in enhancing the exchange between the A and B sites. Since there are no good magnetostructural correlations concerning hydrogen bond mediated spin exchange in low-dimensional magnetic systems, testing of this hypothesis is not possible at this time. However, it must be noted that a series of hydrogen-bonded copper(II) dimers exists where anomalously large exchange-coupling constants were determined ($J = -47.5$ cm^{-1}).[23] In these dimers, the exchange pathway is through a short O-H-O linkage.

Conclusions

The linear-chain series described by $(cat)_2[Mn^{III}(sal)_2(CH_3OH)_2][Mn^{III}(sal)_2]$, provides a system in which the effects of the single-ion anisotropy and exchange interaction without changing the axial or equatorial ligation may be observed. The wide range of magnetic behavior found in this series shows that seemingly small structural changes can have a dramatic impact on the magnetic properties of higher spin chains.

Acknowledgment. This research was supported by NIH Grant GM-39406 (M.S.L., D.P.K., and V.L.P.) and NSF Grant CHE 88-07498 (M.L.K. and W.E.H.). V.L.P. thanks the G. D. Searle Family/Chicago Community Trust for a Biomedical Research Scholar's Award (1986-1989), the Alfred P. Sloan Foundation for a Fellowship (1989-1991), and the Department of Chemistry of the University of North Carolina for their hospitality and a Visiting Professorship.

Supplementary Material Available: For 1-3, Tables VI-XVIII, giving complete experimental crystallographic details, anisotropic thermal parameters of all non-hydrogen atoms, fractional atomic positions for hydrogen atoms, complete bond distances, and complete bond angles, and Figures S1-S5, containing additional magnetic data and complete numbering schemes for all atoms (16 pages); Tables XIX-XXI, listing observed and calculated structure factors (25 pages). Ordering information is given on any current masthead page.

(23) Bertrand, J. A.; Fujita, E.; VanDerveer, D. G. *Inorg. Chem.* **1980**, *19*, 2022.

Contribution from the School of Chemical Sciences and the Beckman Institute, University of Illinois, Urbana—Champaign, Urbana, Illinois 61801

A Molecular Mechanics Model of Ligand Effects. 1. Binding of Phosphites to $Cr(CO)_5$

Mary L. Caffery[1] and Theodore L. Brown*

Received February 21, 1991

Molecular mechanics methods have been employed to compute the minimum energy structures of a series of eight phosphites, including trimethyl phosphite, triethyl phosphite, and triphenyl phosphite, and of their complexes with chromium pentacarbonyl, $Cr(CO)_5$. The MMP2 force field was employed, using the comprehensive computational program BIOGRAF. Substantial changes in lowest energy conformations are seen in the complexes as compared with the free ligands. A major goal of the work was to evaluate the steric contribution to the metal-ligand interaction. As the ligand steric requirement increases, increased van der Waals repulsions between the ligand and the metal carbonyl fragment are largely offset by corresponding increases in van der Waals attractive forces. As a result, neither the overall energy nor net van der Waals interaction energies vary monotonically with increasing ligand steric requirement. The repulsive interactions between the ligand and the metal carbonyl fragment are manifested in bond angle and bond distance changes in the series.

The capacity of ligands, molecules bound to a central metal atom or cluster, to affect the chemical properties of the center is an important consideration in inorganic and organometallic chemistry. Ligand effects are commonly thought to be of two kinds, steric and electronic. Many different approaches have been suggested for separately evaluating these two effects. However, in spite of the substantial attention devoted to this subject, there remains a great deal of uncertainty regarding the best choices of parameters and how they can be best employed in correlating and predicting chemical behavior.

Because of their importance, especially in organometallic systems, phosphorus ligands have been especially throughly studied.[2,3] We will not attempt here to review the enormous

(1) Department of Chemistry, Clarke College, 1550 Clarke Drive, Dubuque, IA 51001-3198.

0020-1669/91/1330-3907$02.50/0